Synergistic Material-Microbe Interface toward Deeper Anaerobic Defluorination

Shun Che[1,2,3,†], Xun Guan[4,†], Roselyn Rodrigues[4,5], Yaochun Yu[1,2,6], Yongchao Xie[4], Chong Liu[4,7,*], Yujie Men[1,2,*]

[1] Department of Chemical and Environmental Engineering, University of California, Riverside, California, 92521, United States

[2] Department of Civil and Environmental Engineering, University of Illinois at Urbana-Champaign, Urbana, Illinois, 61801, United States

[3] SINOPEC Research Institute of Safety Engineering, Qingdao, 266071, People's Republic of China (current address)

[4] Department of Chemistry and Biochemistry, University of California, Los Angeles, California, 90095, United States

[5] College of Arts and Sciences, Gonzaga University, Spokane, WA, 99258, United States (current address)

[6] Department of Environmental Chemistry, Swiss Federal Institute of Aquatic Science and Technology, Dübendorf, Switzerland (current address)

[7] California NanoSystems Institute, University of California Los Angeles, Los Angeles, California 90095, United States

[†] Equal contribution

* Co-corresponding authors: Yujie Men and Chong Liu

Emails: ymen@engr.ucr.edu; chongliu@chem.ucla.edu.

Abstract

Per- and polyfluoroalkyl substances (PFAS), particularly the perfluorinated ones, are recalcitrant to biodegradation. By integrating a reductively defluorinating enrichment culture with biocompatible electrode materials in an electrochemical system, deeper defluorination of a C_6 perfluorinated unsaturated PFAS was achieved compared to the biological or electrochemical system alone. Two types of synergies in the bioelectrochemical system were identified: (i) the microbial-electrochemical in-series defluorination and (ii) the electrochemically enabled microbial defluorination of intermediates at the cathode. Specific cathode microorganisms were enriched, which likely involved in the electrochemically enhanced biodefluorination. The synergies at the material-microbe interface surpassed the limitation of microbial defluorination and further turned the biotransformation end-products into deeper defluorination products, which could be more biodegradable in the environment. It reveals a strong promise of the sustainable material-microbe hybrid system, which could be driven by renewable electricity in PFAS bioremediation and warrants future research to optimize the system and maximize its performance.

Keywords: materials-microbe interface; bioelectrochemical reactors; organofluorines; per- and polyfluoroalkyl substances; defluorination

Significance Statement

Given the incomplete and slow biodegradation of a limited spectrum of per- and polyfluoroalkyl substances (PFAS), this work demonstrated the first endeavor integrating PFAS-degrading microbial communities with state-of-the-art electroactive materials for enhanced bioremediation. It disentangled the synergistic interactions at the material-microbe interface, which promoted the deeper defluorination in the bioelectrochemical system. The findings shed light on the design and optimization of electrochemically driven material-microbe hybrid systems for remediation of PFAS and other halogenated organic pollutants.

Introduction

Integrating electrochemically active materials with microorganisms offers a powerful strategy for creating hybrid biological-inorganic systems and enabling many challenging chemical reactions with high efficiency and selectivity (1-5). By combining the unique reactivities from both electrochemistry and biochemistry, the material-microbe interface integrates the benefits from synthetic and biological catalysts and is proposed to yield new reactivities that were difficult to achieve with either materials or microbes alone (4-7). Evidentially, we demonstrated that such a material-microbe interface is capable of fixing CO_2 and N_2 into chemicals, fuels, and fertilizers, powered by either sunlight or solar electricity, with high efficiencies and reaction throughputs (8-12). Such promising advances propel us to explore new applications and new reactivities with the utilization of material-microbe interface.

One potential application of the material-microbe interface for new reactivity is the defluorination of per- and polyfluoroalkyl substances (PFAS). A large family of over 10,000 manufactured chemicals(13), PFAS have caused severe concerns for public health and ecosystems in recent decades due to their environmental persistence, widespread occurrence, and toxicity (14, 15). While the strong carbon-fluorine (C−F) bonds endow PFAS with extreme chemical and thermal stability for wide applications (16), the same property renders PFAS recalcitrant to environmental degradation and persistent in the environment (17-19). It calls for innovative treatment technologies and remediation strategies. Bioremediation, particularly with naturally occurring microorganisms under environmental conditions, is considered as a more cost-effective and sustainable option for pollutant degradation, including PFAS (20-23). However, such a bioremediation strategy is currently very challenging due to sluggish reactions and incapability of achieving deep and complete defluorination in which an appreciable number of C−F bonds in the molecule are broken with the release of fluoride (F^-) (23, 24). Integrating microbial defluorination with other pathways that complementarily address the challenging degradation steps unachievable by microbes will lead to a synergistic approach that not only keeps the benefits of bioremediation but also offers faster and deeper PFAS defluorination.

We hypothesize that the introduction of electrochemically driven material-microbe interface will address the challenges in PFAS bioremediation and lead to faster and deeper defluorination (Figure. 1A). The synergistic benefits from such an integrated approach could be from two different aspects: First, denoted as the electrochemical effect, the reductive electrochemical driving force on the electrode's surface itself offers additional electrochemical pathways of PFAS decomposition and defluorination; Second, denoted as the bioelectrochemical effect, the presence of electrochemical material-microbe interface may stimulate microbial metabolism (12, 25) and change the species distribution when using microbial consortium for bioremediation, which will lead to completely new reactivities that are unobservable in the electrochemical or microbial system

alone. While those beneficial effects have not been experimentally demonstrated previously, the potential synergy at the material-microbe interface heralds a promising venue of addressing the challenges in bioremediation for faster and deeper PFAS defluorination.

Here we report the observation of faster and deeper PFAS defluorination thanks to the synergy at the electrochemical material-microbe interface. *E*-perfluoro(4-methylpent-2-enoic acid) (PFMeUPA) is one of the two perfluorinated structures reported to be reductively biodefluorinated by commonly available microbial communities, and its biotransformation pathways have been well elucidated (21, 23). With PFMeUPA as a model PFAS molecule, we found that a hybrid system consisting of microbial consortium and biocompatible electrochemical cathode leads to a faster release of F^- from the decomposition of PFMeUPA. Detailed characterization of the transformation products (TPs) during such a process unveils the release of up to 6 F^- per PFMeUPA molecule, a much more significant extent of defluorination than the microbial approach with the release of 1 or 2 F^- per PFMeUPA (23). Moreover, the differences in TP formation between the pure electrochemical system and the electrochemical material-microbe interface indicates the bioelectrochemical effect enabled only at the material-microbe interface. It is corroborated by the observation of an altered distribution of species within the microbial consortium for the hybrid biological-inorganic system. This proof-of-concept study demonstrates a new synergistic strategy taking advantage of both biocatalysis and electrochemistry and opens new avenues of the material-microbe interface for challenging chemical reactions including PFAS degradation and beyond.

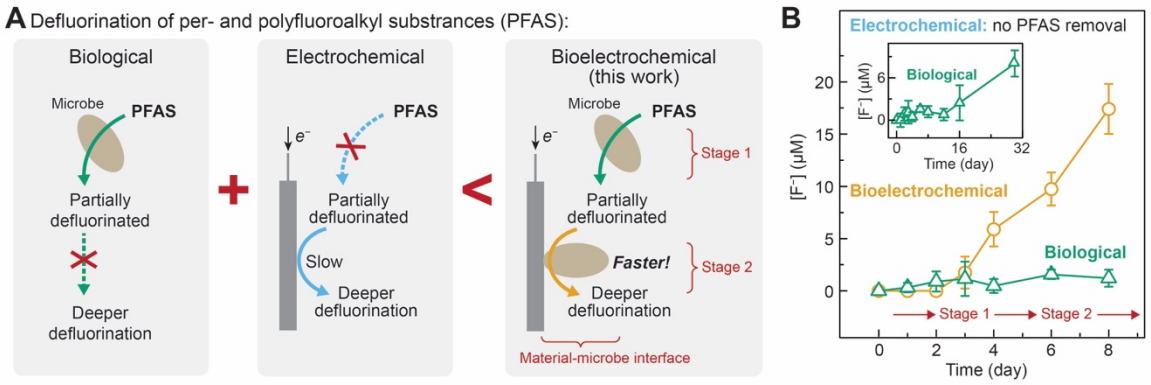

Figure 1. Bioelectrochemical defluorination of PFMeUPA. (A) Scheme of the bioelectrochemical system. (B) Fluoride formation in the bioelectrochemical systems (closed circuit; yellow open circles) and the biological systems (open circuit; green open triangles) performed in triplicates (n = 3, error bars represent standard deviations); the insert figure is the fluoride formation in the biological system with an extended incubation.

Main text

Faster and higher fluoride formation was achieved in the bioelectrochemical system compared to the biological system alone

Previously developed biocompatible cobalt-phosphorus (Co-P) alloy cathode was used in the bioelectrochemical system setup (26, 27) (**Fig. 1A**). Without the inoculation of the defluorinating enrichment culture, the electrochemical system alone did not show any defluorination or degradation of PFMeUPA (**Fig. S1**). However, in the closed-circuit cathodic chamber, when inoculated with the anaerobic enrichment culture capable of reductive defluorination of PFMeUPA, the fluoride formation achieved 17.4 ± 2.4 μM fluoride formation after an eight-day incubation. It was significantly higher than the defluorination (1.2 ± 0.8 μM fluoride formation) in the biological system control, in which H_2 was provided in the headspace (**Fig. 1B**). The biological system started defluorination after a lag phase of two weeks, and it took more than 30 days to reach ~ 9 μM fluoride release (the inserted graph in **Fig. 1B**), which was half of the eight-day defluorination in the bioelectrochemical system.

The significantly higher fluoride release in the bioelectrochemical system was obviously attributed to synergies that occurred at the material-microbe interface. Two types of synergies might be involved: (i) the parent compound or biodefluorination products could be directly defluorinated via electrochemical reactions; (ii) the microbial defluorination could be enhanced at the electricity-driven material-microbe interface. To disentangle which types of synergies contributed to the observed higher defluorination in the bioelectrochemical system, in addition to the bioelectrochemical and biological systems, we further introduced an electrochemical system inoculated with the spent medium of the same defluorinating enrichment culture as inoculated in the bioelectrochemical and biological systems. The spent medium was cell-free but contained the transformation products of PFMeUPA, extracellular enzymes and secreted biomolecules from the culture. The same amount of PFMeUPA was amended in the bioelectrochemical, electrochemical, and biological systems (**Fig. 2A**). By comparing the fluoride formation and analyzing the parent compound and transformation products (TPs), we demonstrated the occurrence of the two types of synergies that led to the significantly higher defluorination in the bioelectrochemical system. In the following two sections, we described and interpreted the detailed results indicating the two types of synergies at the electrochemically driven material-microbe interface.

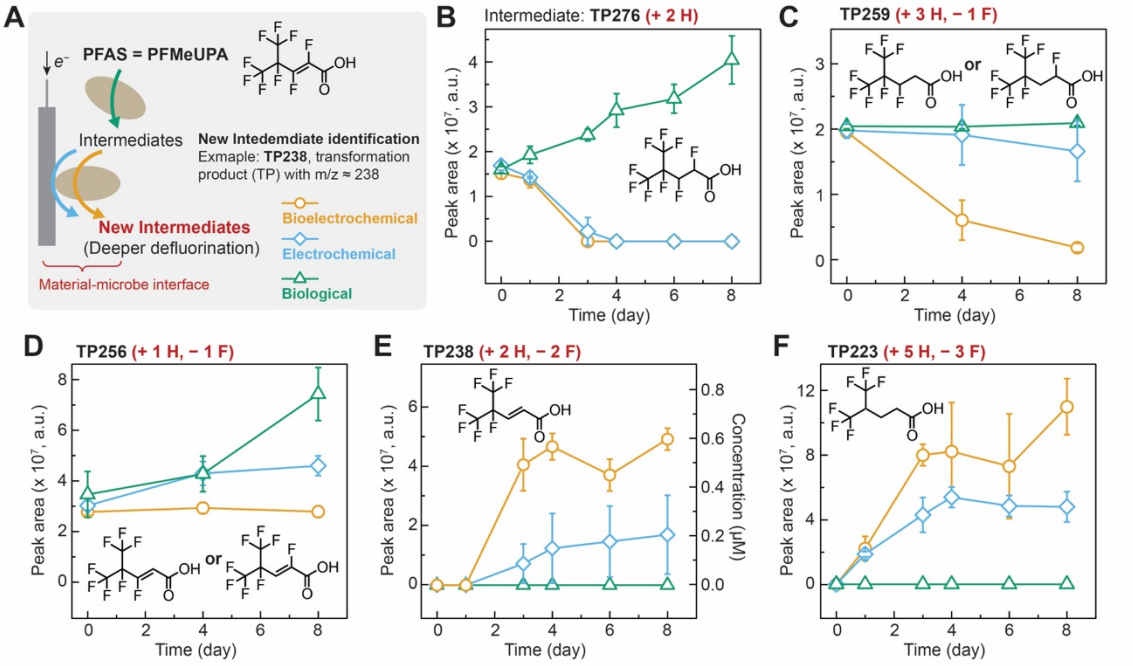

Figure 2. Bioelectrochemical defluorination products. (A) Defluorination processes at the materials-microbe interface (bioelectrochemical: yellow open circles; electrochemical: blue open diamonds; biological: green open triangles). (B) – (F) formation of the major transformation products (TPs), TP276, 259, 256, 238, and 223 (see the chromatographs, MS and MS^2 spectra in **Fig. S3**), in the biological, electrochemical, and bioelectrochemical systems (Note: n = 3, and error bars represent standard deviations; despite no PFMeUPA addition or culture/spent medium inoculation in the anodic chamber, a slight diffusion of PFMeUPA and some TPs were observed from the cathodic to the anodic chamber. Thus, the total concentration or peak areas detected in both chambers were used in the plots.)

Synergy 1: Electrochemical defluorination of PFMeUPA biotransformation products

According to the identified TPs, we elucidated the plausible transformation pathways of PFMeUPA in the electrochemical system. Although the electrochemical system alone did not show any removal of the parent compound PFMeUPA (**Fig. S2A**), it still exhibited fluoride formation (**Fig. S2B**). This was attributed to the electrochemical defluorination of the biotransformation products of PFMeUPA carried over from the spent medium. It indicates the first type of synergy at the material-microbe interface in the bioelectrochemical system, which led to deeper defluorination as the parent compound was microbially transformed to the electrochemically degradable TPs (**Fig. 3A**).

In the electrochemical system, one major carry-over biological end-product, TP276 (via the biological hydrogenation of PFMeUPA) (23), was rapidly degraded (**Fig. 2B**) likely via reductive defluorination forming TP259 and via HF elimination forming TP256 (**Fig. 2 C&D** and **Fig. 3B**).

TP259, another major end-product of PFMeUPA biotransformation (23), was further defluorinated via HF elimination, corresponding to the formation of a structurally confirmed intermediate, TP238, in the electrochemical system (**Fig. 2C**, **E**, and **Fig. 3A**). Subsequently, several deeper defluorination TPs were formed likely from the further transformation of TP238 (**Fig. 2F** and **Fig. 4B**). We confirmed the electrochemical defluorination of TP238 by spiking its reference standard into the same electrochemical system. The same TPs (i.e., TP241, TP223, TP205, TP200, and TP169 in **Fig. 3B**) as those detected in the electrochemical system spiked with PFMeUPA were formed from the electrochemical degradation of TP238 (**Fig. S5**).

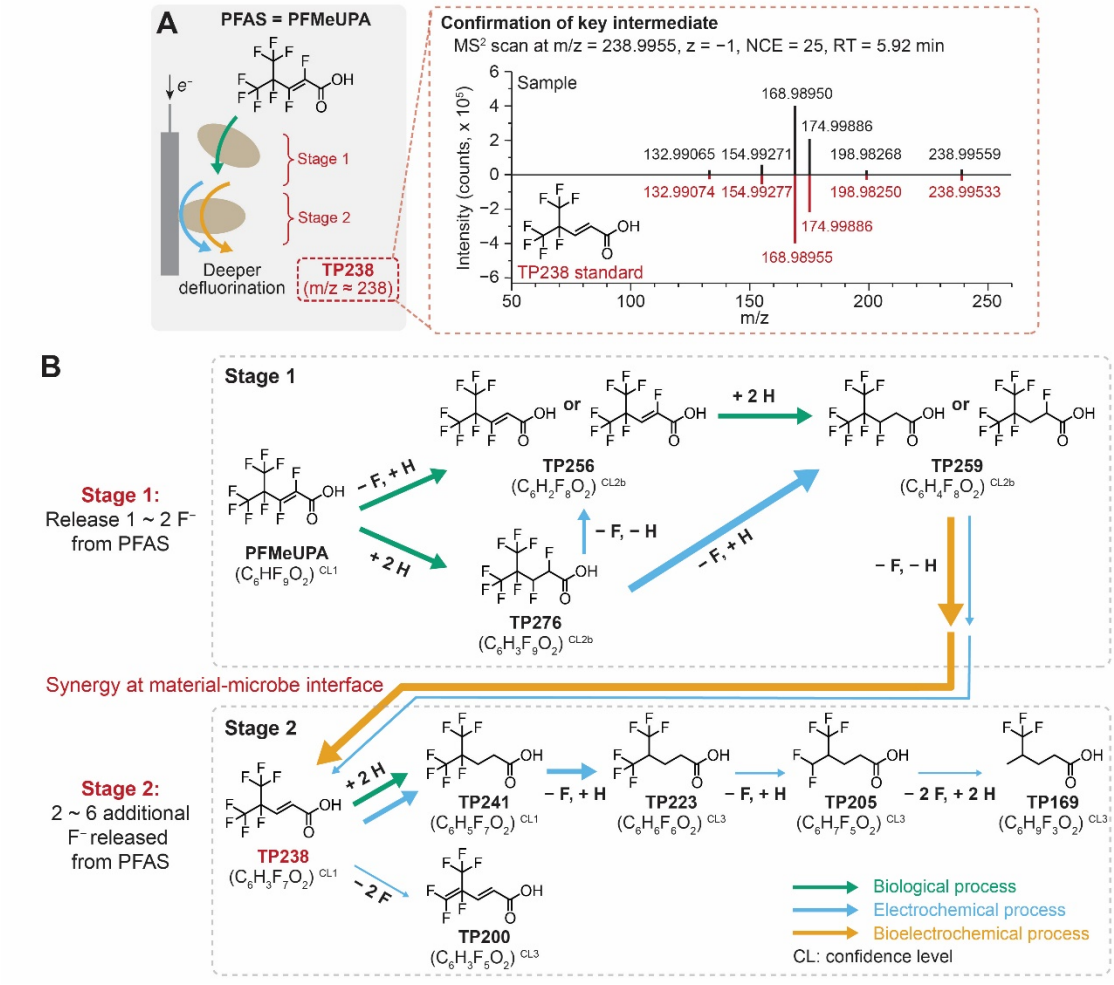

Figure 3. **PFMeUPA defluorination pathways at the electrochemically driven material-microbe interface.** (A) Validation of TP238 structure by comparing the retention times and MS^2 profiles between the experimental sample and the reference standard, 4,5,5,5-tetrafluoro-4-(trifluoromethyl)-2- pentenoic acid. (B) Proposed PFMeUPA biotransformation pathways in the biological, electrochemical, and bioelectrochemical systems (CL: confidence level determined

according to the criteria by Schymanski *et al*. (28); the thickness of arrows indicates the relative contributions of the reactions to the transformation; the text next to each arrow indicates the changes in formula from PFMeUPA; see **Fig. S4** regarding the formation curves of the deeper defluorination products, i.e., TP241, TP205, TP200, and TP169).

In the biological system, TP276 (from hydrogenation, +2H from PFMeUPA) and TP259 (from the hydrogenation of the reductive defluorination intermediate TP256, -F+H+2H from PFMeUPA) were the two major end-products from the anaerobic biotransformation of PFMeUPA (23). The integration with the electrochemical system surpasses the microbial limitation and breaks down those two biological end-products of PFMeUPA into less fluorinated TPs, none of which could be formed biologically alone. Thus, the biological transformation of PFMeUPA into TP276 and TP259 coupled with the subsequent electrochemical transformation of those biotransformation TPs was the first type of synergy leading to the deeper defluorination in the bioelectrochemical system.

Synergy 2: Electrochemically enhanced/enabled microbial transformation

Besides the synergy via electrochemical transformation of the biotransformation end-products of PFMeUPA, we observed the second type of synergy at the material-microbe interface in the bioelectrochemical system, where some biotransformation processes were electrochemically enhanced, leading to faster parent compound removal and fluoride formation. First, since the parent compound, PFMeUPA was only transformed biologically (**Fig. 3B**), its faster removal observed in the bioelectrochemical system than in the biological system (**Fig. S2A**) suggested an enhanced PFMeUPA biotransformation via a more efficient electron transfer at the electricity-driven material-microbe interface. Similarly, the further biotransformation of TP256 (**Fig. 3B**) was enhanced in the bioelectrochemical system because the level of TP256 in the bioelectrochemical system was lower than that in the biological and electrochemical systems, where TP256 was accumulated (**Fig. 2D**).

On top of the electrochemically enhanced biological transformations, we also observed electrochemically enabled biodefluorination of some intermediates, which cannot occur in the biological system alone. It included the HF elimination of TP259 forming TP238 and the formation of TP223 from TP238. Compared to the electrochemical system alone, the bioelectrochemical system achieved a much faster removal of TP259, corresponding to the same faster formation trend of TP238 (**Fig. 2C** and **E**). Thus, in addition to the electrochemical conversion, microbial transformation of TP259 to TP238 was also involved (**Fig. 3B**), which was only enabled in the bioelectrochemical system, because in the biological system alone TP259 was a stable end-product and cannot be biotransformed (23). Microbially, TP238 was transformed into the end-product TP241 via hydrogenation without further degradation (23). In comparison, in the bioelectrochemical system, TP238 was further transformed resulting in the formation of the

192 downstream less fluorinated TPs, TP205, TP200, and TP169, which was mostly attributed to
193 electrochemical defluorination (**Fig. 3B**) as no significant differences in the formation were
194 observed between the electrochemical system and the bioelectrochemical system (**Fig. S4**).
195 The electrochemically enhanced and enabled biological processes suggested that specific
196 microbial groups could be selected in the bioelectrochemical system. We conducted the 16S rRNA
197 gene amplicon sequencing to examine changes in the composition of microbial communities in the
198 cathodic chamber of the bioelectrochemical system and in the biological system (**Fig. 4A**). Microbial
199 groups enriched in the bioelectrochemical system were likely involved in the
200 biotransformation/defluorination steps enhanced or enabled by the applied electricity. The microbial
201 community was divided into two groups: one was attached to the cathode material, and the other
202 was in the culture suspension (**Fig. 4A**). The microbial distribution in cathode-attached and
203 suspended communities was analyzed separately in the bioelectrochemical and biological
204 systems.

205 In the biological system with the addition of the same cathode material, microbial growth
206 was observed both on the surface of the cathode material and in the culture suspension. There
207 were no significant differences in the distribution of the abundant taxonomic groups between the
208 attached and planktonic growth, except that TAXA4 (*Desulfovirga*-like) and the methanogenic
209 TAXA6 (*Methanosaeta*-like) had better growth in suspension (**Fig. 4B**). Compared to the biological
210 system, microorganisms mostly grew on the cathode in the bioelectrochemical system. A very little
211 amount of genomic DNA was extracted from the cells collected from the culture suspension, and
212 only one out of the four replicates retrieved sufficient DNA for the sequencing analysis, which had
213 a similar taxonomic distribution as the cathode-associated community (**Fig. 4B**). Thus, we used the
214 cathode-associated community to represent the microbial community growing in the
215 bioelectrochemical system. It exhibited a substantial difference in community composition from that
216 in the biological system (**Fig. 4B**), which was also reflected in the SEM images (**Fig. S6**). One
217 specific taxonomic group (TAXA1) in the genus *Clostridium* showed an outgrowth on the cathode
218 with the electricity applied than without (80% vs. 29%). Meanwhile, the most dominant taxonomic
219 group in the biological system, TAXA2 (an unspecified *Clostridiales* family bacterium), was
220 outcompeted to extinction in the bioelectrochemical system. Although TAXA1 and TAXA2 were the
221 closest among all abundant taxonomies (> 1% in relative abundance), they were still low in the 16S
222 rRNA gene similarity (87.5%) (**Fig. 4C**) and seemed to be quite different in physiological
223 characteristics and electroactive properties. A number of *Clostridium* species such as *Clostridium*
224 *cochlearium*, *Clostridium butyricum, Clostridium ljungdahlii*, and *Clostridium aceticum* have been
225 reported to be electroactive in bioelectrochemical systems (29-31). Microorganisms whose growth
226 could benefit from the excess H_2 generated from the cathodic chamber may also be selected. It
227 suggests that the TAXA1 *Clostridium* species were capable of direct electron transfer or efficient

utilization of H_2, thus were likely involved in the electrochemically enhanced/enabled biotransformation/defluorination steps, such as the removal of the parent compound and the formation of less fluorinated TP238. The characterization of TAXA1 microorganisms and the molecular mechanisms of biotransformation/defluorination warrants further investigation in follow-up studies.

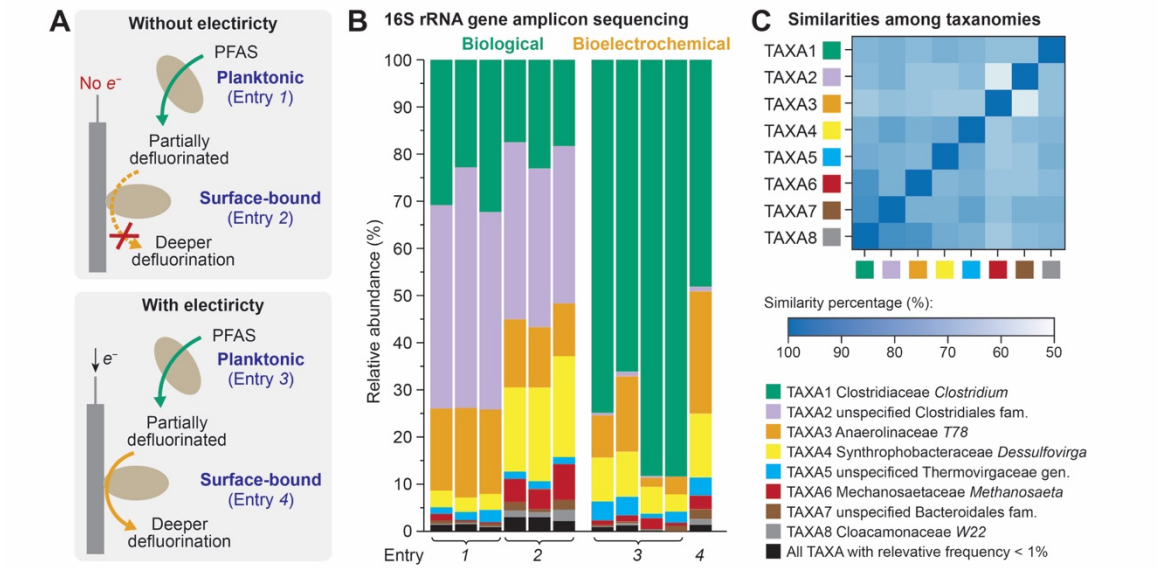

Figure 4. **Community shift in the bioelectrochemical system.** (A) Sample entries investigated by the 16S rRNA gene amplicon sequencing; (B) The top eight taxa with > 1% relative abundance according to the 16S rRNA gene amplicon sequencing analysis. The assigned taxonomic classification is listed as family name followed by genus name; (C) Similarity among the top eight taxa identified in the microbial communities (see the phylogenetic distribution of OTUs in the eight taxa in **Fig. S5**).

Discussion

Faster and deeper defluorination of PFMeUPA was achieved by an electricity-driven material-microbe system compared to the biodefluorination by the microorganisms alone. Two types of synergies in the bioelectrochemical system were identified. In the cathodic chamber with a closed circuit, the material-microbe hybrid system generated less fluorinated TPs, which were not formed in the biological system alone. Those TPs were from further defluorination of the two major biotransformation products of PFMeUPA via electrochemical reactions. Some TPs could also be formed via deeper microbial defluorination that could not occur in the biological system but were enabled at the electrochemically driven material-microbe interface. According to the detected TPs,

the bioelectrochemical system could achieve up to six F^- release from the parent compound, much higher than the slightly more than one F^- release via pure microbial processes (23). One should note that the transformation of PFMeUPA could only be realized by microbial processes. Thus, ensuring continuous biodegradation of PFMeUPA, in other words, sustained growth of the degrading microorganisms in the bioelectrochemical system, is pivotal to achieving deeper defluorination. Despite the enhanced biotransformation rate of PFMeUPA in the bioelectrochemical system, the decrease in microbial activities likely caused the decrease in PFMeUPA degradation F^- formation, hence the decoupling of the PFMeUPA biodegradation from the faster degradation of its biotransformation products. Nonetheless, by optimizing the growth conditions of PFMeUPA-degrading microorganisms, selecting more efficient defluorinating microbial species, and developing more biocompatible electrode materials, sustainable and robust microbial growth and further enhanced PFMeUPA biotransformation kinetics could be achieved, leading to complete transformation of PFMeUPA with a higher defluorination degree through the two types of synergies in the bioelectrochemical system.

The synergies at the electricity-driven material-microbe interface promote versatility and create new capacities for the bioremediation of PFAS. In the biological system, the reductive defluorination and hydrogenation reactions are two competing anaerobic pathways. The hydrogenation pathway generates microbially stable end-products and hinders further defluorination. Since the two pathways might be carried out by the same microorganisms, it would be difficult to specifically inhibit the hydrogenation pathway. Here, we proved that this obstacle could be overcome by the integrating defluorinating microorganisms with a biocompatible electrochemical system, as it showed rapid degradation and defluorination of the two stable end-products formed from the biological hydrogenation pathway. Compared to the biological system that only worked with specific unsaturated structures, the bioelectrochemical system exhibited higher versatility in the reactive structures, implying a higher potential for degrading saturated fluorinated structures. Although the parent compound was still not fully mineralized, the deeper bioelectrochemical defluorination resulted in end-products with more C–H bonds, which may be less toxic and more vulnerable to aerobic biodegradation. Some commonly occurring aerobic microorganisms may be able to further degrade and defluorinate those cathode end-products (21, 24, 32, 33), and this could be even simultaneously realized in the O_2-generating anodic chamber if the cathode solution could be periodically transferred into the anodic chamber.

Electrolysis has been investigated and even applied for bioremediation, providing O_2 for aerobic microorganisms or H_2 for anaerobic microorganisms in the degradation of various pollutants (34-39). This electrochemical approach could be more sustainable by using electricity generated from solar panels in the field (40). Here, we demonstrated the potential of a novel electricity-driven material-microbe hybrid system in achieving deeper defluorination using a model

biodegradable perfluorinated compound. With more defluorinating microorganisms and the responsible enzymes being identified, the same electrochemical system could be integrated with different forms of biocatalysts to improve the destruction performance. The discovered synergies at the material-microbe interface could also be applied to many other PFAS compounds that showed sluggish biotransformation, as well as other halogenated contaminants to facilitate enhanced reductive dehalogenation.

Methods

Chemicals

Standard compounds of (E)-perfluoro(4-methylpent-2-enoic acid)(denoted "PFMeUPA", CAS number:103229-89-6) and 4,5,5,5-tetrafluoro-4-(trifluoromethyl)-2- pentenoic acid (CAS number: 243139-64-2) were purchased from SynQuest Laboratories (Alachua, FL). A 10 mM stock solution of each standard was prepared in autoclaved anaerobic Milli-Q water in a 160-mL sealed serum bottle and stored at room temperature until use.

Cultures and Growth Conditions

The defluorinating enrichment originated from KB-1® generously provided by SiREM Lab (https://www.siremlab.com/) and has been maintained in Dr. Men's lab since 2017. All cultures were maintained in 160-mL sealed serum bottles containing 100 mL of a sterile anaerobic basal medium with 100 µg/L vitamin B_{12} as previously described and an H_2 headspace (**Table S1**) (41, 42). PFMeUPA (~70 µM) was added as the external electron acceptor and readded upon depletion. All cultures were incubated at 34 °C in a dark incubator without shaking.

Electrode Plating

The CoPi and Co-P alloy electrodes were prepared by electrochemical deposition, following the previously reported method (22). The electrochemical deposition was conducted in a three-electrode system with a working electrode of electrode substrate, a counter electrode of Pt wire (CH Instrument CHI115), and a reference electrode of Ag/AgCl (1 M KCl) (CH Instrument CHI111P) with the Gamry Interface 1000E potentiostat. The deposition solution of CoPi electrode contains 10 mM $Co(NO_3)_2$ and 0.1 M methylphosphonate (MePi) buffer (pH 8). The carbon cloth (Fuel Cell Earth CC6P40) that was sequentially rinsed with acetone and DI water was applied as electrode substrates. The deposition was performed at 0.85 V vs. reference until 500 mC/cm^2 charge was passed. The deposition solution of CoP electrode contains 0.15 M H_3BO_3, 0.1 M NaCl, 0.33 M $Na_2H_2PO_2$, and 0.2 M $CoCl_2$. The stainless mesh (AlfaFisher 45002-CH) that was sequentially rinsed with acetone and DI water was applied as electrode substrates. The deposition was performed at −1.2 V vs. reference for 15 min.

Bioelectrochemical System Setup

Experiments of bulk electrolysis were conducted in a custom-made two-chamber glass electrochemical cell (Adams and Chittenden Scientific Glass). It had two 150-ml chambers separated by a Nafion 117 membrane (Sigma-Aldrich 274674-1). The experiments were run in parallel using an eight-channel Gamry Interface 1000E potentiostat interfaced with a Gamry ECMB multiplexer. The incubation temperature was 30 °C, which was maintained by a water bath with constant stirring of 150 rpm under a pure N_2 gas atmosphere. The working electrode was a stainless-steel mesh electrodeposited with CoP alloy catalyst (see "Electrode Plating"), the counter electrode was the carbon cloth electrodeposited with CoPi catalyst (see "Electrode Plating"), and the reference electrode was the leak-free Ag/AgCl reference electrode (Innovative Instruments, Inc. LF-1-100). The cathodic chamber was flushed with pure N_2 gas, then 95 ml modified BAV1 medium containing ~70 μM PFMeUPA was transferred anaerobically into the cathodic chamber. The reducing agent was added as needed to maintain the anaerobic condition. Then, in the triplicated bioelectrochemical system, 5 ml of the living culture was injected into the cathodic chamber to make the final electrolysis suspension/solution. The anodic chamber contained 100 ml modified BAV1 medium only. Multiplexed chronoamperometry was performed on the reactors under the selected voltage that would yield the targeted current densities (~ 1 mA/cm^2). The electrochemical system was set up in triplicates in the same way as the bioelectrochemical system, except that 5 mL spent medium (0.22 μm filtrate of the living culture) was inoculated into the cathodic chamber instead of the living culture. The biological system was set up in triplicates by inoculating 5 mL living culture into 160-mL sealed serum bottles containing 95 mL modified BAV1 medium, H_2 headspace, and the same cathode material used in the bioelectrochemical system. The addition of the cathode material in the biological system was to examine its effect on microbial activities and the microbes attached to it.

A 2-ml liquid from the cathodic and anodic chambers of the bioelectrochemical and electrochemical systems, as well as the biological system, was taken by syringes on day 0, 1, 2, 3, 4, 6, and 8. The samples were centrifugated at 13,000 rpm for 15 min at 4ºC. The supernatant was stored at 4ºC for F^-, parent compound, and transformation product analyses, while the cell pellets were kept at –20 ºC for the 16S rRNA gene amplicon sequencing. At the end of the experiment, the cathode material in the bioelectrochemical and biological systems was taken out and stored at –20 ºC for the 16S rRNA gene amplicon sequencing.

Potential adsorption of PFMeUPA and its transformation products (TPs) (i.e., TP276, TP256, and TP259) was tested (Supplemental Methods), and no adsorption was observed. Fluoride and other anionic compounds were rejected by the cation-exchange membrane and not detected in the anodic chamber, except PFMeUPA, TP256, and TP259. A modified SPE protocol

(Supplemental Methods) was applied to extract those compounds from the anodic samples to remove the salts. Total peak areas of samples from both chambers were reported for those compounds.

Fluoride-Ion Measurement by the Ion-Selective Electrode Method

Fluoride ion was measured using an ion-selective electrode (ISE) (HACH). The detection limit was 0.02 mg/L (ca. 1 μM). The fluoride measurement by ISE was previously cross-validated using ion chromatography (23).

High-Performance Liquid Chromatography Coupled to High-Resolution Tandem Mass Spectrometry Analysis

The parent PFAS compounds and TPs were analyzed by an Ultra-high performance liquid chromatography coupled to a high-resolution quadrupole orbitrap mass spectrometer (UHPLC-HRMS/MS, Q Exactive, Thermo Fisher Scientific, Waltham, MA). Two μL sample was injected into a Hypersil Gold column (particle size 1.9 μm, 2.1×100 mm, Thermo Fisher Scientific) and eluted at 0.30 mL/min with water (A) and methanol (B), each containing 10 mM ammonium acetate. The linear gradient was: 95% A for 0 – 1 min, 5% A for 6 – 8 min, and 95% A for 8 – 10 min. Samples were analyzed by a full scan (m/z 50 – 750) at a resolution of 140,000 (m/z 200) under the negative electrospray ionization mode. The suspect and non-target screening procedure was described in the Supplemental Methods.

16S rRNA Gene Amplicon Sequencing Analysis

Genomic DNA was extracted from the biomass growing in suspension and attached to the cathode material in both the bioelectrochemical and biological systems. The DNA samples was sent to Laragen (Culver, CA) for 16S rRNA gene amplicon sequencing using MiSeq PE250. The primers targeting the V3-4 region of the 16S rRNA gene were used, i.e., forward primer: CCTACGGGNGGCWGCAG and reverse primer: GACTACHVGGGTATCTAATCC. Sequences were analyzed on the microbiome bioinformatics platform QIIME 2 v2022.2 (https://qiime2.org/). Raw sequences were first imported into QIIME 2 and subject to assembly, quality control (with a minimum quality score of 25), and feature table construction using DADA2. The obtained amplicon sequencing variances were further clustered into operational taxonomic units (OTUs) with a minimum of 99% similarity. The most abundant sequence was automatically selected as the representative sequence for each specific OTU. The closest taxonomy (TAXA) at the genus level was assigned to each OTU using gg-13-8-99-515-806-nb-classifier. Each TAXA may contain multiple OTUs (**Table S2** and **Fig. S5**) due to the low resolution of the taxonomic level.

Data Accession Numbers

The 16S rRNA amplicon sequencing raw reads were deposited to the National Center for Biotechnology Information (NCBI) BioProject (https://www.ncbi.nlm.nih.gov/bioproject) under the accession number PRJNA913546.

Acknowledgments

This study was supported by NIEHS (Award No. R01ES032668, for S.C., R.R., X.G., C.L., and Y.M.) and SERDP (Project No. ER20-1541, for Y.Y. and Y.M.).

References

1. D. K. Dogutan, D. G. Nocera, Artificial Photosynthesis at Efficiencies Greatly Exceeding That of Natural Photosynthesis. *Acc. Chem. Res.* 10.1021/acs.accounts.9b00380 (2019).
2. N. Kornienko, J. Z. Zhang, K. K. Sakimoto, P. Yang, E. Reisner, Interfacing nature's catalytic machinery with synthetic materials for semi-artificial photosynthesis. *Nat. Nanotechnol.* **13**, 890-899 (2018).
3. K. K. Sakimoto, N. Kornienko, P. Yang, Cyborgian Material Design for Solar Fuel Production: The Emerging Photosynthetic Biohybrid Systems. *Acc. Chem. Res.* **50**, 476-481 (2017).
4. H. Chen, F. Dong, S. D. Minteer, The progress and outlook of bioelectrocatalysis for the production of chemicals, fuels and materials. *Nature Catalysis* **3**, 225-244 (2020).
5. T. Zhang, More efficient together. *Science* **350**, 738-739 (2015).
6. S. Cestellos-Blanco, H. Zhang, J. M. Kim, Y.-x. Shen, P. Yang, Photosynthetic semiconductor biohybrids for solar-driven biocatalysis. *Nature Catalysis* **3**, 245-255 (2020).
7. K. P. Nevin, T. L. Woodard, A. E. Franks, Z. M. Summers, D. R. Lovley, Microbial Electrosynthesis: Feeding Microbes Electricity To Convert Carbon Dioxide and Water to Multicarbon Extracellular Organic Compounds. *mBio* **1** (2010).
8. C. Liu, B. C. Colón, M. Ziesack, P. A. Silver, D. G. Nocera, Water Splitting-Biosynthetic System with CO2 reduction Efficiencies Exceeding Photosynthesis. *Science* **352**, 1210-1213 (2016).
9. C. Liu, K. K. Sakimoto, B. C. Colón, P. A. Silver, D. G. Nocera, Ambient nitrogen reduction cycle using a hybrid inorganic–biological system. *Proc. Natl. Acad. Sci. U. S. A.* **114**, 6450-6455 (2017).
10. R. M. Rodrigues *et al.*, Perfluorocarbon nanoemulsion promotes the delivery of reducing equivalents for electricity-driven microbial CO2 reduction. *Nature Catalysis* **2**, 407-414 (2019).
11. S. Lu, X. Guan, C. Liu, Electricity-Powered Artificial Root Nodule. *Nat. Commun.* **11**, 1505 (2020).
12. X. Guan *et al.*, Maximizing light-driven CO2 and N2 fixations in biology-material hybrids. *Nature Catalysis* (2022).
13. S. J. Barnabas *et al.*, Extraction of Chemical Structures from Literature and Patent Documents using Open Access Chemistry Toolkits: A Case Study with PFAS. *Digital Discovery* 10.1039/D2DD00019A (2022).
14. M. G. Evich *et al.*, Per- and polyfluoroalkyl substances in the environment. *Science* **375**, eabg9065 (2022).

15. Z. Y. Wang, J. DeWitt, C. P. Higgins, I. T. Cousins, A never-ending story of per- and polyfluoroalkyl substances (PFASs)? . *Environ. Sci. Technol.* **52**, 3325-3325 (2018).
16. J. Gluge *et al.*, An overview of the uses of per- and polyfluoroalkyl substances (PFAS). *Environ Sci Process Impacts* **22**, 2345-2373 (2020).
17. C. J. Young *et al.*, Perfluorinated acids in Arctic snow: new evidence for atmospheric formation. *Environ. Sci. Technol.* **41**, 3455-3461 (2007).
18. F. Xiao, Emerging poly- and perfluoroalkyl substances in the aquatic environment: A review of current literature. *Water Res.* **124**, 482-495 (2017).
19. K. Rankin, S. A. Mabury, T. M. Jenkins, J. W. Washington, A North American and global survey of perfluoroalkyl substances in surface soils: Distribution patterns and mode of occurrence. *Chemosphere* **161**, 333-341 (2016).
20. L. P. Wackett, Nothing lasts forever: understanding microbial biodegradation of polyfluorinated compounds and perfluorinated alkyl substances. *Microb. Biotechnol.* **n/a** (2021).
21. Y. Yu *et al.*, Microbial defluorination of unsaturated per- and polyfluorinated carboxylic acids under anaerobic and aerobic conditions: A structure specificity study. *Environ. Sci. Technol.* **56**, 4894-4904 (2022).
22. P. L. McCarty, C. S. Criddle, T. M. Vogel, Retrospective on microbial transformations of halogenated organics. *Environ Sci Process Impacts* **22**, 512-517 (2020).
23. Y. Yu *et al.*, Microbial cleavage of C-F bonds in two C_6 per- and polyfluorinated compounds via reductive defluorination. *Environ Sci Technol* **54**, 14393-14402 (2020).
24. J. Liu, S. Mejia Avendano, Microbial degradation of polyfluoroalkyl chemicals in the environment: a review. *Environ. Int.* **61**, 98-114 (2013).
25. R. Zhang *et al.*, Proteomic and Metabolic Elucidation of Solar-Powered Biomanufacturing by Bio-Abiotic Hybrid System. *Chem* **6**, 234-249 (2020).
26. C. Liu, B. C. Colon, M. Ziesack, P. A. Silver, D. G. Nocera, Water splitting-biosynthetic system with CO_2 reduction efficiencies exceeding photosynthesis. *Science* **352**, 1210-1213 (2016).
27. D. A. Lutterman, Y. Surendranath, D. G. Nocera, A self-healing oxygen-evolving catalyst. *J. Am. Chem. Soc.* **131**, 3838-3839 (2009).
28. E. L. Schymanski *et al.*, Identifying small molecules via high resolution mass spectrometry: communicating confidence. *Environ. Sci. Technol.* **48**, 2097-2098 (2014).
29. L. Schwab, L. Rago, C. Koch, F. Harnisch, Identification of Clostridium cochlearium as an electroactive microorganism from the mouse gut microbiome. *Bioelectrochemistry* **130**, 107334 (2019).

30. H. S. Park *et al.*, A novel electrochemically active and Fe (III)-reducing bacterium phylogenetically related to Clostridium butyricum isolated from a microbial fuel cell. *Anaerobe* **7**, 297-306 (2001).
31. K. P. Nevin *et al.*, Electrosynthesis of organic compounds from carbon dioxide is catalyzed by a diversity of acetogenic microorganisms. *Appl. Environ. Microbiol.* **77**, 2882-2886 (2011).
32. S. Che *et al.*, Structure-Specific Aerobic Defluorination of Short-Chain Fluorinated Carboxylic Acids by Activated Sludge Communities. *Environ. Sci. Technol. Lett.* **8**, 668-674 (2021).
33. N. Wang *et al.*, Aerobic biotransformation of ^{14}C-labeled 8-2 telomer alcohol by activated sludge from a domestic sewage treatment plant. *Environ. Sci. Technol.* **39**, 531-538 (2005).
34. S. T. Lohner, A. Tiehm, Application of electrolysis to stimulate microbial reductive PCE dechlorination and oxidative VC biodegradation. *Environ. Sci. Technol.* **43**, 7098-7104 (2009).
35. X. Wang *et al.*, Microbial electrochemistry for bioremediation. *Environmental Science and Ecotechnology* **1**, 100013 (2020).
36. F. Yan, D. Reible, Electro-bioremediation of contaminated sediment by electrode enhanced capping. *J. Environ. Manage.* **155**, 154-161 (2015).
37. D. B. Gent, A. H. Wani, J. L. Davis, A. Alshawabkeh, Electrolytic redox and electrochemical generated alkaline hydrolysis of hexahydro-1,3,5-trinitro-1,3,5 triazine (RDX) in sand columns. *Environmental science & technology* **43**, 6301-6307 (2009).
38. J. A. Franz, R. J. Williams, J. R. V. Floraa, M. E. Meadows, W. G. Irwin, Electrolytic oxygen generation for subsurface delivery: effects of precipitation at the cathode and an assessment of side reactions. *Water Res.* **36**, 2243-2254 (2002).
39. C. L. Chun, R. B. Payne, K. R. Sowers, H. D. May, Electrical stimulation of microbial PCB degradation in sediment. *Water Res.* **47**, 141-152 (2013).
40. E. M. Nichols *et al.*, Hybrid bioinorganic approach to solar-to-chemical conversion. *Proceedings of the National Academy of Sciences* **112**, 11461-11466 (2015).
41. Y. J. Men *et al.*, Sustainable syntrophic growth of *Dehalococcoides ethenogenes* strain 195 with *Desulfovibrio vulgaris* Hildenborough and *Methanobacterium congolense*: global transcriptomic and proteomic analyses. *ISME J.* **6**, 410-421 (2012).
42. J. He, V. F. Holmes, P. K. Lee, L. Alvarez-Cohen, Influence of vitamin B_{12} and cocultures on the growth of Dehalococcoides isolates in defined medium. *Appl Environ Microbiol* **73**, 2847-2853 (2007).